Supplemental Material:

Supplemental Figure 1. Quantile-Quantile Plot of associations of single nucleotide polymorphisms with relative slope of eGFR, among (A) cross-ancestry analyses, (B) White participants and (C) Black participants.

Supplemental Figure 2. Regional interrogation of the *UMOD/PDILT* locus, cross-ancestry analysis. Plot shows -log10(p-value) on the left Y-axis and genomic location (in base pairs) on the X-axis. Pairwise linkage disequilibrium, r-squared, between the top lead genetic variant (shown as a dark purple circle) and the surrounding variants is expressed using a gradient, detailed in the top right-hand corner of the plot. Known genes are presented below the plot as arrows, indicating the location and size, as well as the direction of transcription, of each gene. Genetic variants which are not in LD of any of significant independent lead variants in the selected region are colored grey. CADD (Combined Annotation Dependent Depletion) score, a tool for scoring the deleteriousness of single nucleotide variants as well as insertion/deletions variants in the human genome (cadd.gs.washington.edu), with higher scores indicating a higher likelihood of being deleterious. Only variants which are in LD of any of significant independent lead variants are displayed in the plot. RegulomeDB rank computed based on the integration of multiple high-throughput datasets, including functional genomics features along with continuous values such as ChIP-seq signal, DNase-seq signal, information content change, and DeepSEA scores among others (regulomedb.org). Only variants which are in LD of any of significant independent lead variants are displayed in the plot.

Supplemental Figure 3. Regional interrogation of the *UMOD/PDILT* locus among Black participants. Plot shows -log10(p-value) on the left Y-axis and genomic location (in base pairs) on the X-axis. Lead genetic variant is shown as a dark purple diamond. Known genes are presented below the plot as arrows, indicating the location and size, as well as the direction of transcription, of each gene.

Supplemental Figure 4. Comparison between longitudinal and cross-sectional eGFR data. Correlation between the meta-analysis results using current data and CKD-GEN and UKBioBank eGFR creatinine GWAS data (PMID 34272381), p-values (A) and beta estimates (B).

Supplemental Figure 5. Regional interrogation of the *BICC1* locus, cross-ancestry analysis. Plot shows -log10(p-value) on the left Y-axis and genomic location (in base pairs) on the X-axis. Pairwise linkage disequilibrium, r-squared, between the top lead genetic variant (shown as a dark purple circle) and the surrounding variants is expressed using a gradient, detailed in the top right-hand corner of the plot. Known genes are presented below the plot as arrows, indicating the location and size, as well as the direction of transcription, of each gene. Genetic variants which are not in LD of any of significant independent lead variants in the selected region are colored grey. CADD (Combined Annotation Dependent Depletion) score, a tool for scoring the deleteriousness of single nucleotide variants as well as insertion/deletions variants in the human genome (cadd.gs.washington.edu), with higher scores indicating a higher likelihood of being deleterious. Only variants which are in LD of any of significant independent lead variants are displayed in the plot. RegulomeDB rank computed based on the integration of multiple high-

throughput datasets, including functional genomics features along with continuous values such as ChIP-seq signal, DNase-seq signal, information content change, and DeepSEA scores among others (regulomedb.org). Only variants which are in LD of any of significant independent lead variants are displayed in the plot.

Supplemental Figure 6. Regional interrogation of the *APOL1* locus among Black participants. Plot shows -log10(p-value) on the left Y-axis and genomic location (in base pairs) on the X-axis. Pairwise linkage disequilibrium, r-squared, between the top lead genetic variant (shown as a dark purple circle) and the surrounding variants is expressed using a gradient, detailed in the top right-hand corner of the plot. Known genes are presented below the plot as arrows, indicating the location and size, as well as the direction of transcription, of each gene. Genetic variants which are not in LD of any of significant independent lead variants in the selected region are colored grey. CADD (Combined Annotation Dependent Depletion) score, a tool for scoring the deleteriousness of single nucleotide variants as well as insertion/deletions variants in the human genome (cadd.gs.washington.edu), with higher scores indicating a higher likelihood of being deleterious. Only variants which are in LD of any of significant independent lead variants are displayed in the plot. RegulomeDB rank computed based on the integration of multiple high-throughput datasets, including functional genomics features along with continuous values such as ChIP-seq signal, DNase-seq signal, information content change, and DeepSEA scores among others (regulomedb.org). Only variants which are in LD of any of significant independent lead variants are displayed in the plot.

Supplemental Figure 7. Regional interrogation of the *UMOD/PDILT* locus, cross-ancestry analysis among individuals with diabetes. Plot shows -log10(p-value) on the left Y-axis and genomic location (in base pairs) on the X-axis. Lead genetic variant is shown as a dark purple diamond. Pairwise linkage disequilibrium, r-squared, between the top lead genetic variant (shown as a dark purple circle) and the surrounding variants is expressed using a gradient, detailed in the top right-hand corner of the plot. Known genes are presented below the plot as arrows, indicating the location and size, as well as the direction of transcription, of each gene.

Supplemental Figure 8. Regional interrogation of the *HEATR4* locus among Black individuals with diabetes. Plot shows -log10(p-value) on the left Y-axis and genomic location (in base pairs) on the X-axis. Lead genetic variant is shown as a dark purple diamond. Pairwise linkage disequilibrium, r-squared, between the top lead genetic variant (shown as a dark purple circle) and the surrounding variants is expressed using a gradient, detailed in the top right-hand corner of the plot. Known genes are presented below the plot as arrows, indicating the location and size, as well as the direction of transcription, of each gene.

Supplemental Figure 9. Regional interrogation of the *UMOD/PDILT* locus from transethnic analyses among individuals without diabetes. Plot shows -log10(p-value) on the left Y-axis and genomic location (in base pairs) on the X-axis. Lead genetic variant is shown as a dark purple diamond. Pairwise linkage disequilibrium, r-squared, between the top lead genetic variant (shown as a dark purple circle) and the surrounding variants is expressed using a gradient, detailed in the top right-hand corner of the plot. Known genes are presented below the plot as arrows, indicating the location and size, as well as the direction of transcription, of each gene.

Supplemental Figure 10. Regional interrogation of the *BICC1* locus from cross-ancestry analyses among individuals without diabetes. Plot shows -log10(p-value) on the left Y-axis and genomic location (in base pairs) on the X-axis. Lead genetic variant is shown as a dark purple diamond. Pairwise linkage disequilibrium, r-squared, between the top lead genetic variant (shown as a dark purple circle) and the surrounding variants is expressed using a gradient, detailed in the top right-hand corner of the plot. Known genes are presented below the plot as arrows, indicating the location and size, as well as the direction of transcription, of each gene.

Supplemental Figure 11. Regional interrogation of the *PRKAG2* locus from cross-ancestry analyses. Plot shows -log10(p-value) on the left Y-axis and genomic location (in base pairs) on the X-axis. Lead genetic variant is shown as a dark purple diamond. Known genes are presented below the plot as arrows, indicating the location and size, as well as the direction of transcription, of each gene.

Supplemental Figure 12. Regional interrogation of the *FGF5* locus from cross-ancestry analyses. Plot shows -log10(p-value) on the left Y-axis and genomic location (in base pairs) on the X-axis. Lead genetic variant is shown as a dark purple diamond. Known genes are presented below the plot as arrows, indicating the location and size, as well as the direction of transcription, of each gene.

Supplemental Figure 13. Regional interrogation of the *C15ORF54* locus from cross-ancestry analyses. Plot shows -log10(p-value) on the left Y-axis and genomic location (in base pairs) on the X-axis. Lead genetic variant is shown as a dark purple diamond. Known genes are presented below the plot as arrows, indicating the location and size, as well as the direction of transcription, of each gene.

Supplemental Figure 14. Violin plots of distribution of relative eGFR by *APOL1* inheritance model among Black participants without (A) and with (B) diabetes. The boxes indicate the 75th (upper horizontal line), mean + SEM (black bold horizontal line), median (white dot), and the 25th (lower horizontal line), percentiles of the distribution. The upper whiskers indicate the maximum value of inverse normally transformed relative eGFR slope located within a distance of 1.5 times the interquartile range above the 75th percentile. The lower whiskers indicate the corresponding distance to the 25th percentile value. Surrounding the boxes (colored area) on each side is a rotated kernel density plot, which is comparable to a histogram with infinitely small bin sizes. The left-hand panels present the violin plots for *APOL1* according to a recessive inheritance pattern, which presumes an identical risk profile for individuals with 0 or 1 high-risk alleles. The right-hand panels present the violin plots for *APOL1* according to an additive inheritance pattern, which presumes a stepwise additional risk per high-risk allele.

Supplemental Figure 15. Manhattan plot of the strength of association of genetic variants with eGFR decline (%/year) among White individuals with chronic kidney disease. Y-axis represents –log10 p-value for linear mixed model of genetic variant dosage on repeated log-transformed eGFR measurements, adjusted for age, sex and first 10 principal components of ancestry, stratified by diabetes at baseline among White individuals, then meta-analyzed for diabetes-adjusted results. X-axis indicates the chromosomal position of each SNP. A dotted red line marks the $p=1\times10^{-8}$ threshold.

Supplemental Figure 16. Manhattan plot of the strength of association of genetic variants with eGFR decline (%/year) among Black individuals with chronic kidney disease. Y-axis represents –log10 p-value for linear mixed model of genetic variant dosage on repeated log-transformed eGFR measurements, adjusted for age, sex and first 10 principal components of ancestry, stratified by diabetes at baseline among Black individuals, then meta-analyzed diabetes-adjusted results. X-axis indicates the chromosomal position of each SNP. A dotted red line marks the $p=1\times10^{-8}$ threshold.

Supplemental Table 1. Associations of single nucleotide polymorphisms with relative slope of eGFR, cross-ancestry analyses ($p<5 \times 10^{-8}$). All genetic variants with $p<5 \times 10^{-8}$ for linear mixed model of genetic variant dosage on repeated log-transformed eGFR measurements, adjusted for age, sex and first 10 principal components of ancestry, stratified by diabetes at baseline and race/ethnicity, then meta-analyzed for cross-ancestry results.
Supplemental Table 1.xls

Supplemental Table 2. Associations of single nucleotide polymorphisms with relative slope of eGFR, among White individuals ($p<5 \times 10^{-6}$). All genetic variants with $p<5 \times 10^{-6}$ for linear mixed model of genetic variant dosage on repeated log-transformed eGFR measurements among White participants, adjusted for age, sex and first 10 principal components of ancestry, stratified by diabetes at baseline, then meta-analyzed for cross-ancestry results.
Supplemental Table 2.xls

Supplemental Table 3. Associations of single nucleotide polymorphisms with relative slope of eGFR, among Black individuals ($p<5 \times 10^{-6}$). All genetic variants with $p<5 \times 10^{-6}$ for linear mixed model of genetic variant dosage on repeated log-transformed eGFR measurements among Black participants, adjusted for age, sex and first 10 principal components of ancestry, stratified by diabetes at baseline, then meta-analyzed for cross-ancestry results.
Supplemental Table 3.xls

Supplemental Table 4. Associations of independent genetic variants with relative slope of eGFR in Gorski et al. summary statistics (PMID 35716955). Independent genetic variants that were significantly associated with the relative slope phenotype in our analyses were searched for in the summary statistics of the Gorski et al. manuscript (PMID 35716955) and resulting beta estimates and p-values are displayed.

Supplemental Table 5. Associations of single nucleotide polymorphisms with relative slope of eGFR, among individuals with diabetes, cross-ancestry analyses ($p<5 \times 10^{-6}$). All genetic variants with $p<5 \times 10^{-6}$ for linear mixed model of genetic variant dosage on repeated log-transformed eGFR measurements among individuals with diabetes at baseline, adjusted for age, sex and first 10 principal components of ancestry, stratified by race/ethnicity then meta-analyzed for cross-ancestry results.
Supplemental Table 5.xls

Supplemental Table 6. Associations of single nucleotide polymorphisms with relative slope of eGFR, among White individuals with diabetes ($p<5 \times 10^{-6}$). All genetic variants with $p<5 \times 10^{-6}$

for linear mixed model of genetic variant dosage on repeated log-transformed eGFR measurements among White individuals with diabetes at baseline, adjusted for age, sex and first 10 principal components of ancestry.
Supplemental Table 6.xls

Supplemental Table 7. Associations of single nucleotide polymorphisms with relative slope of eGFR, among Black individuals with diabetes ($p<5 \times 10^{-6}$). All genetic variants with $p<5 \times 10^{-6}$ for linear mixed model of genetic variant dosage on repeated log-transformed eGFR measurements among Black individuals with diabetes at baseline, adjusted for age, sex and first 10 principal components of ancestry.
Supplemental Table 7.xls

Supplemental Table 8. Associations of single nucleotide polymorphisms with absolute slope of eGFR, among individuals with diabetes, cross-ancestry analyses ($p<5 \times 10^{-6}$). All genetic variants with $p<5 \times 10^{-6}$ for linear mixed model of genetic variant dosage on repeated eGFR measurements among individuals with diabetes at baseline, adjusted for age, sex and first 10 principal components of ancestry, stratified by race/ethnicity then meta-analyzed for cross-ancestry results.
Supplemental Table 8.xls

Supplemental Table 9. Associations of single nucleotide polymorphisms with absolute slope of eGFR, among White individuals with diabetes ($p<5 \times 10^{-6}$). All genetic variants with $p<5 \times 10^{-6}$ for linear mixed model of genetic variant dosage on repeated eGFR measurements among White individuals with diabetes at baseline, adjusted for age, sex and first 10 principal components of ancestry.
Supplemental Table 9.xls

Supplemental Table 10. Associations of single nucleotide polymorphisms with absolute slope of eGFR, among Black individuals with diabetes ($p<5 \times 10^{-6}$). All genetic variants with $p<5 \times 10^{-6}$ for linear mixed model of genetic variant dosage on repeated log-transformed eGFR measurements among Black individuals with diabetes at baseline, adjusted for age, sex and first 10 principal components of ancestry.
Supplemental Table 10.xls

Supplemental Table 11. Associations of single nucleotide polymorphisms with relative slope of eGFR, among individuals without diabetes, cross-ancestry analyses ($p<5 \times 10^{-6}$). All genetic variants with $p<5 \times 10^{-6}$ for linear mixed model of genetic variant dosage on repeated log-transformed eGFR measurements among individuals without diabetes at baseline, adjusted for age, sex and first 10 principal components of ancestry, stratified by race/ethnicity then meta-analyzed for cross-ancestry results.
Supplemental Table 11.xls

Supplemental Table 12. Associations of single nucleotide polymorphisms with relative slope of eGFR, among White individuals without diabetes ($p<5 \times 10^{-6}$). All genetic variants with $p<5 \times 10^{-6}$ for linear mixed model of genetic variant dosage on repeated log-transformed eGFR

measurements among White individuals without diabetes at baseline, adjusted for age, sex and first 10 principal components of ancestry.
Supplemental Table 12.xls

Supplemental Table 13. Associations of single nucleotide polymorphisms with relative slope of eGFR, among Black individuals without diabetes ($p<5 \times 10^{-6}$). All genetic variants with $p<5 \times 10^{-6}$ for linear mixed model of genetic variant dosage on repeated log-transformed eGFR measurements among Black individuals without diabetes at baseline, adjusted for age, sex and first 10 principal components of ancestry.
Supplemental Table 13.xls

Supplemental Table 14. Associations of single nucleotide polymorphisms with absolute slope of eGFR, among individuals without diabetes, cross-ancestry analyses ($p<5 \times 10^{-6}$). All genetic variants with $p<5 \times 10^{-6}$ for linear mixed model of genetic variant dosage on repeated eGFR measurements among individuals without diabetes at baseline, adjusted for age, sex and first 10 principal components of ancestry, stratified by race/ethnicity then meta-analyzed for cross-ancestry results.
Supplemental Table 14.xls

Supplemental Table 15. Associations of single nucleotide polymorphisms with absolute slope of eGFR, among White individuals without diabetes ($p<5 \times 10^{-6}$). All genetic variants with $p<5 \times 10^{-6}$ for linear mixed model of genetic variant dosage on repeated eGFR measurements among White individuals without diabetes at baseline, adjusted for age, sex and first 10 principal components of ancestry.
Supplemental Table 15.xls

Supplemental Table 16. Associations of single nucleotide polymorphisms with absolute slope of eGFR, among Black individuals without diabetes ($p<5 \times 10^{-6}$). All genetic variants with $p<5 \times 10^{-6}$ for linear mixed model of genetic variant dosage on repeated eGFR measurements among Black individuals without diabetes at baseline, adjusted for age, sex and first 10 principal components of ancestry.
Supplemental Table 16.xls

Supplemental Table 17. Association of *APOL1* high-risk variants with eGFR slope among Black individuals without diabetes at baseline. Black participants with 2 G1 alleles, or 1 G1 and 1 G2 alleles were classified as *APOL1* high-risk and those with only 1 G1 or G2 allele or no G1 or G2 alleles were defined as *APOL1* low-risk.
Supplemental Table 17.xls

Supplemental Table 18. Association of *APOL1* high-risk variants with eGFR slope among Black individuals with diabetes at baseline. Black participants with 2 G1 alleles, or 1 G1 and 1 G2 alleles were classified as *APOL1* high-risk and those with only 1 G1 or G2 allele or no G1 or G2 alleles were defined as *APOL1* low-risk.
Supplemental Table 18.xls

MVP core acknowledgements: Acknowledgment of the Million Veteran Program leadership and staff contributions can be found in the supplementary material entitled.

Supplemental Figure 1. Quantile-Quantile Plot of associations of single nucleotide polymorphisms with relative slope of eGFR, among (A) cross-ancestry analyses, (B) White participants and (C) Black participants

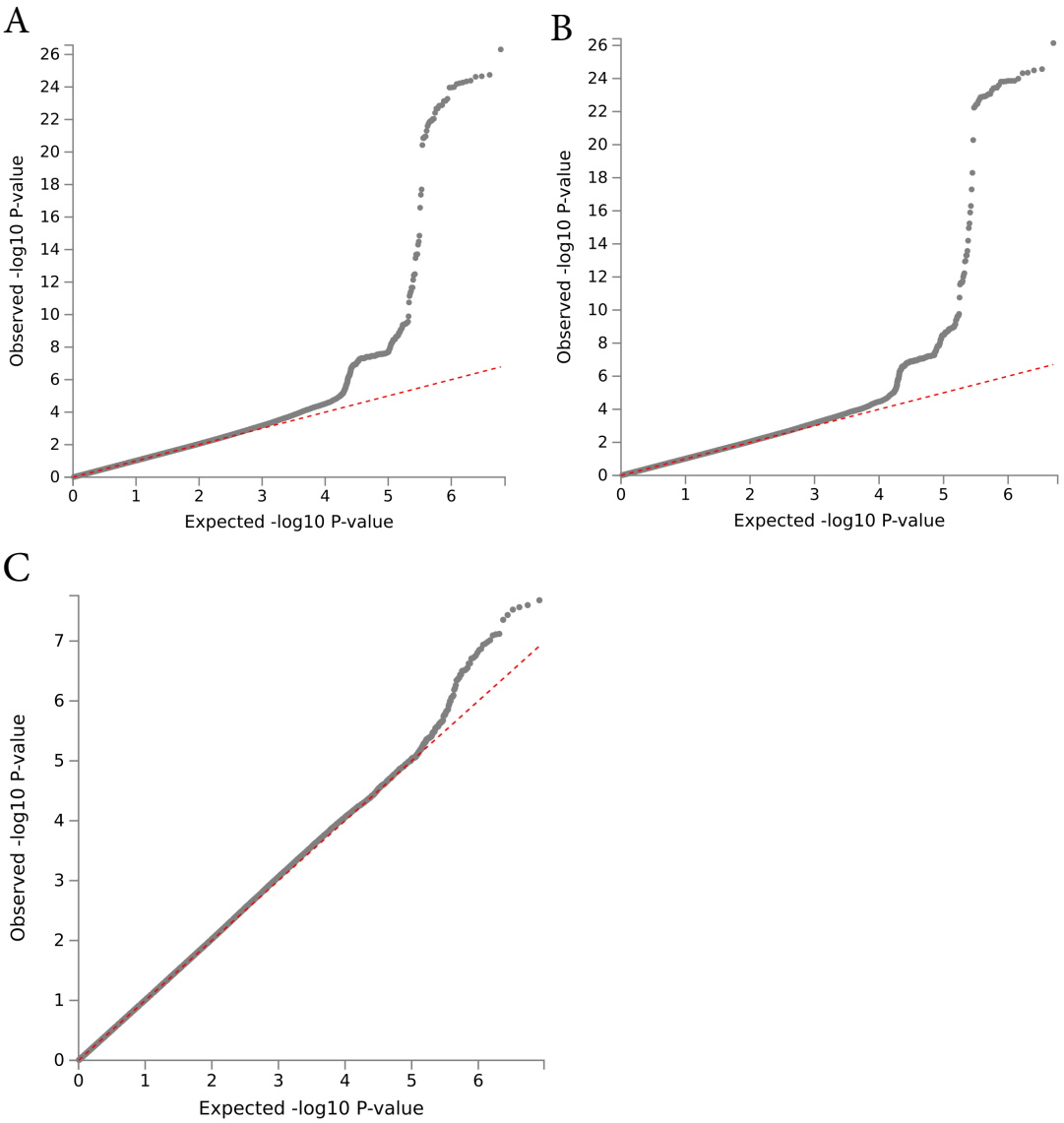

Supplemental Figure 2. Regional interrogation of the *UMOD/PDILT* locus, cross-ancestry analysis

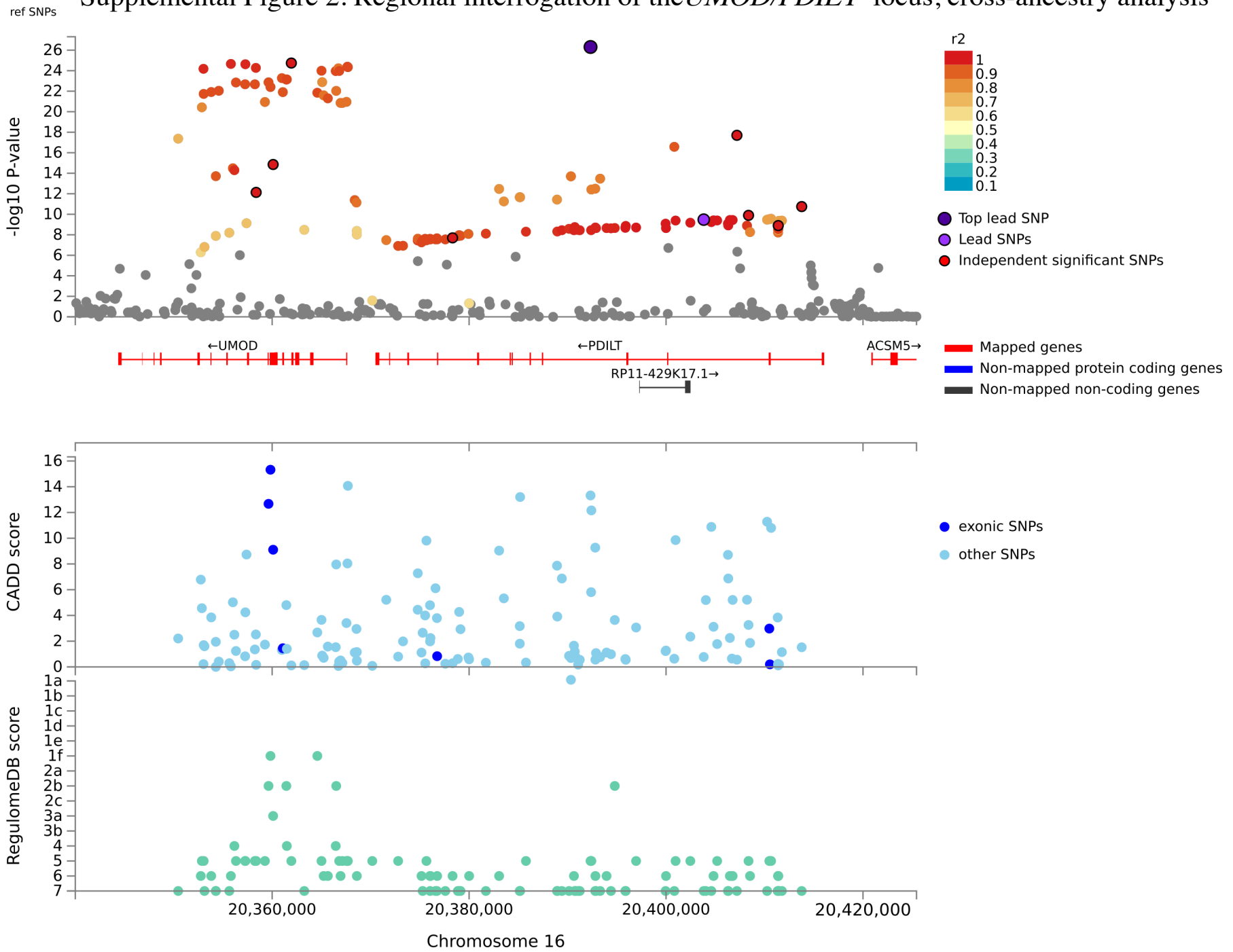

Supplemental Figure 3. Regional interrogation of the UMOD/PDILT locus among Black participants.

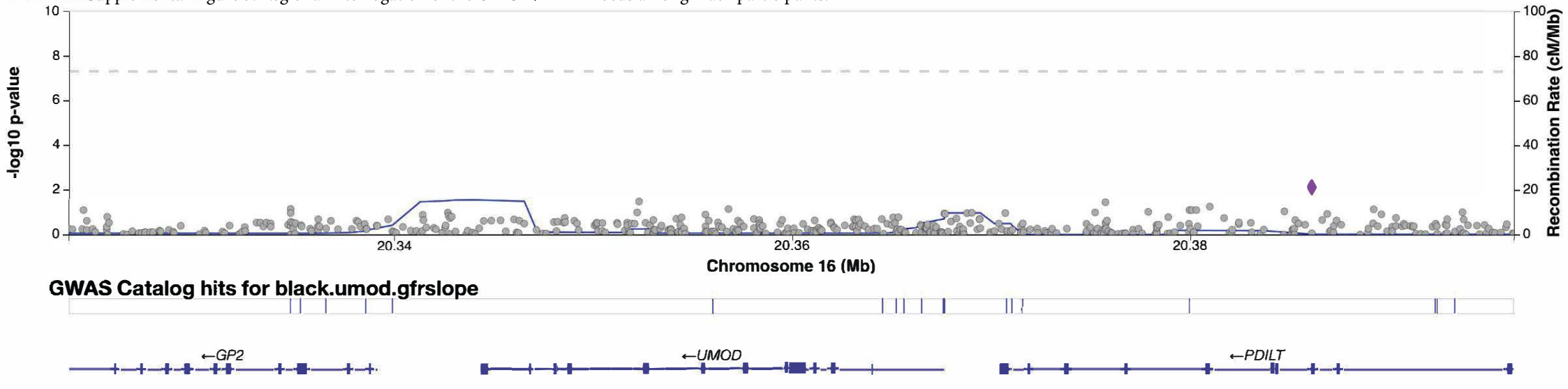

Supplemental Figure 4. Comparison between longitudinal and cross-sectional eGFR data. Correlation between the meta-analysis results using current data and CKD-GEN and UKBioBank eGFR creatinine GWAS data (PMID 34272381), p-values (A) and beta estimates (B).

A.

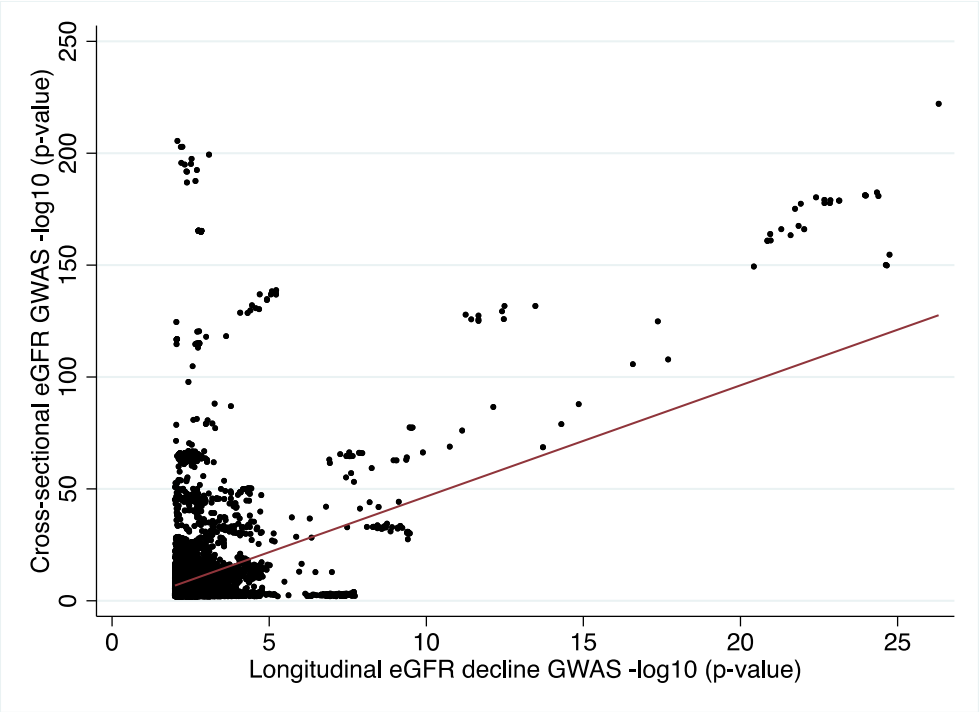

B.

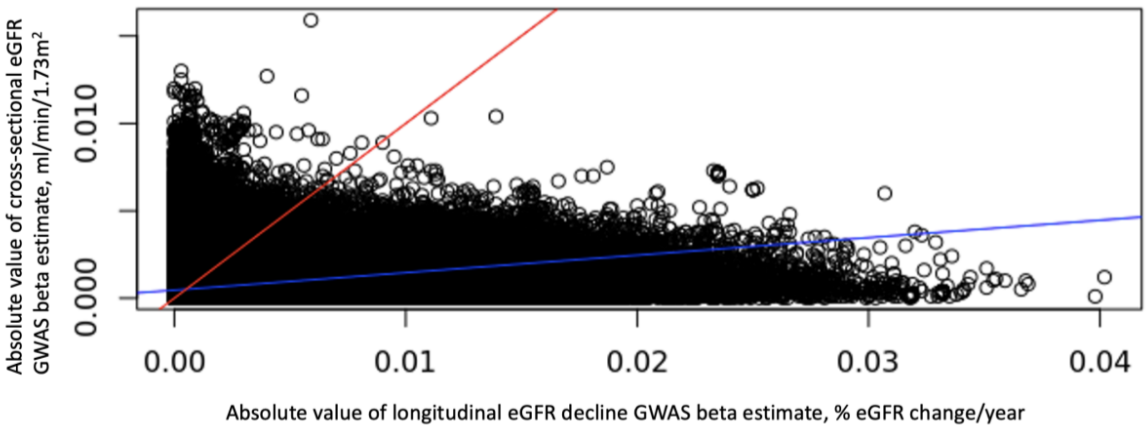

Supplemental Figure 5. Regional interrogation of the BICC1 locus, cross-ancestry analysis

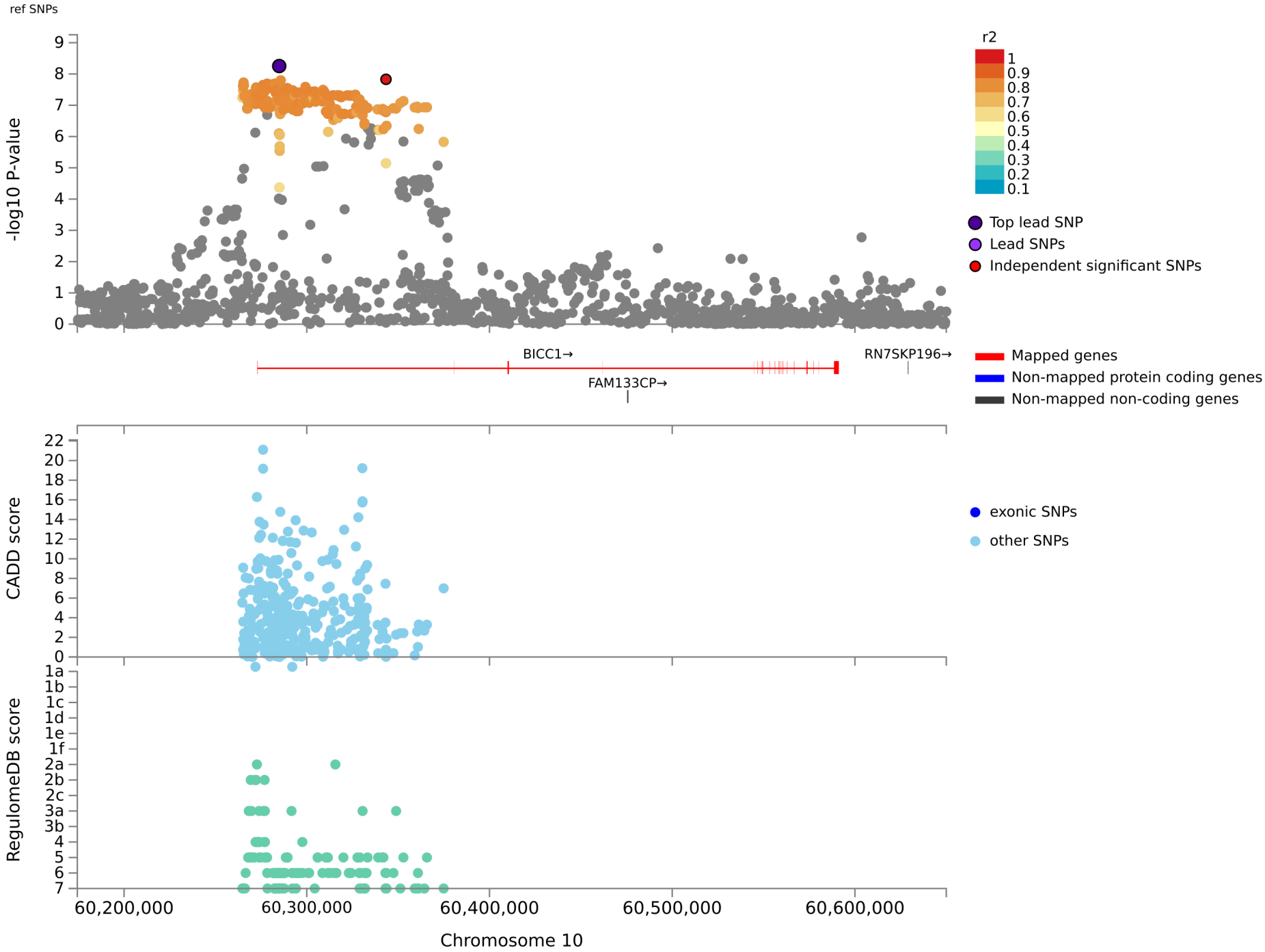

Supplemental Figure 6. Regional interrogation of the *APOL1* locus among Black participants

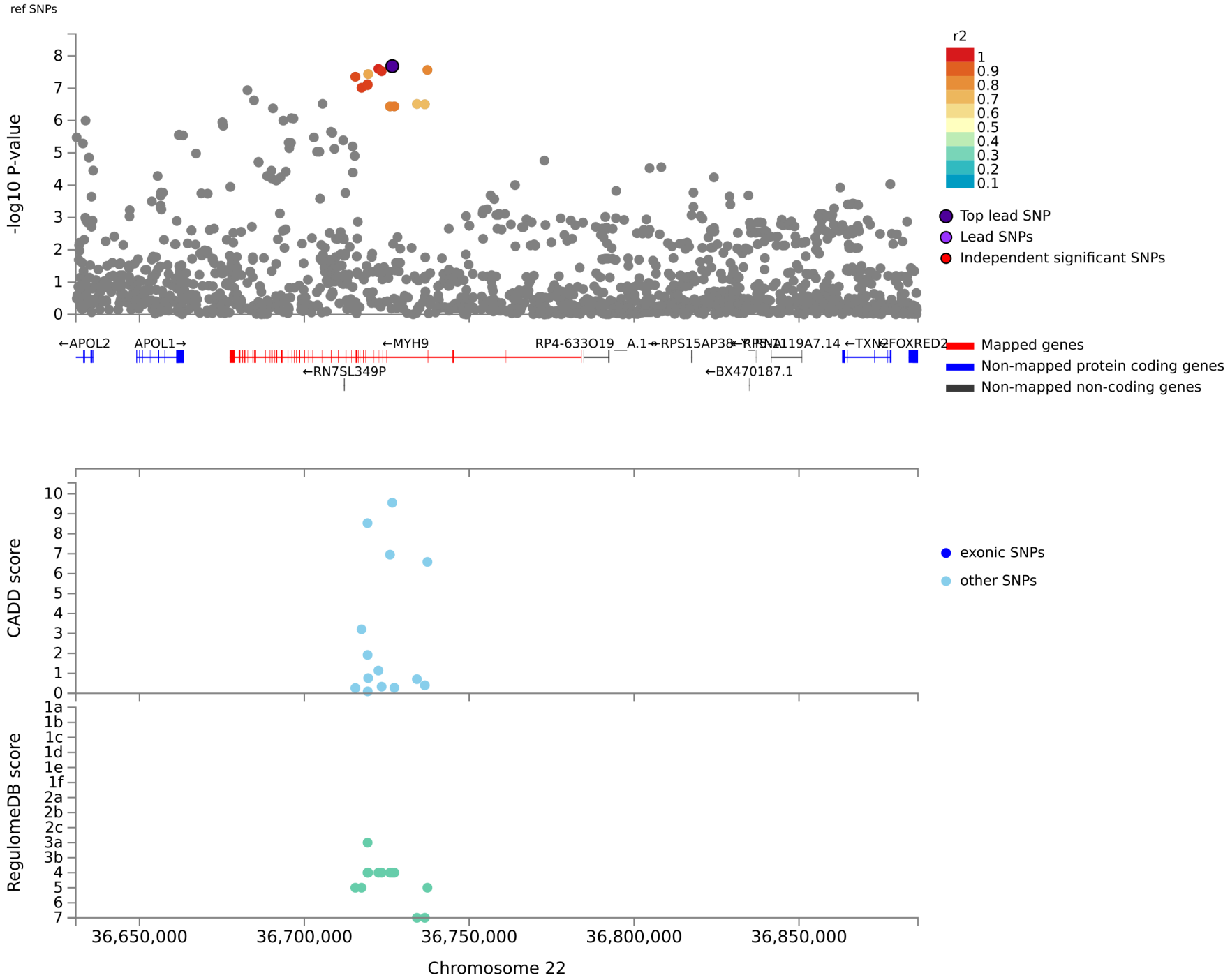

Supplemental Figure 7. Regional interrogation of the *UMOD/PDILT* locus, cross-ancestry analysis among individuals with diabetes

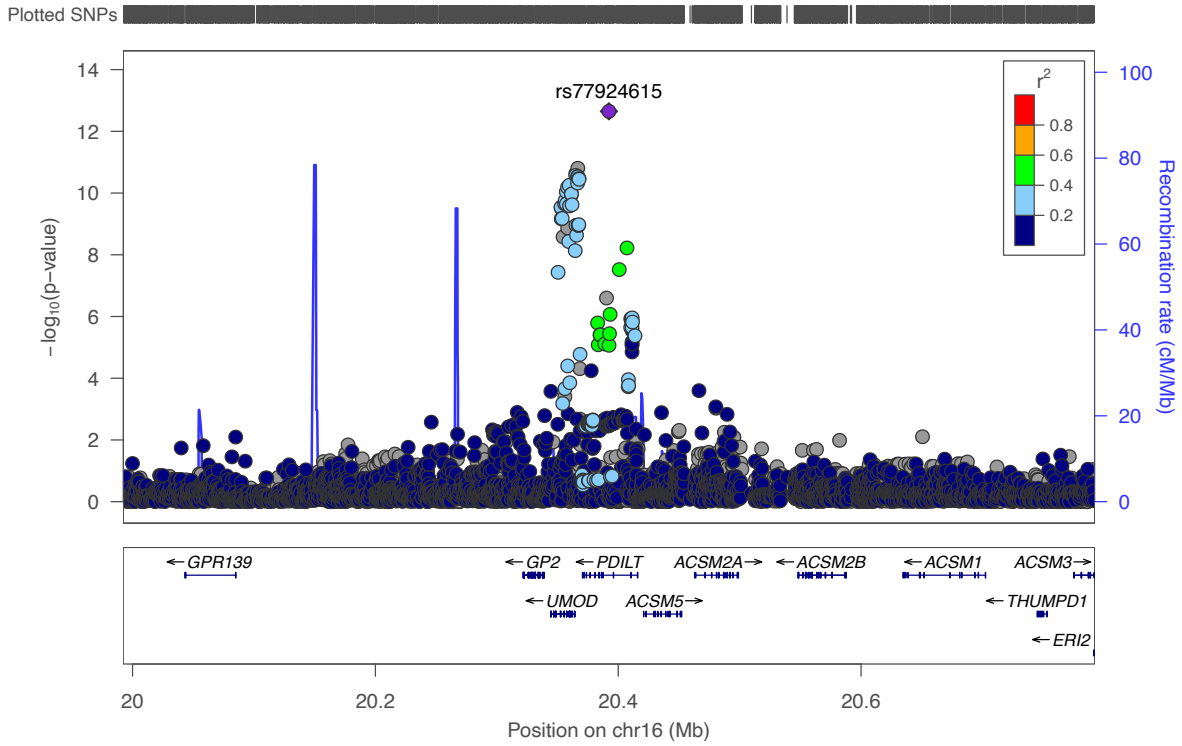

Supplemental Figure 8. Regional interrogation of the *HEATR4* locus among Black individuals with diabetes

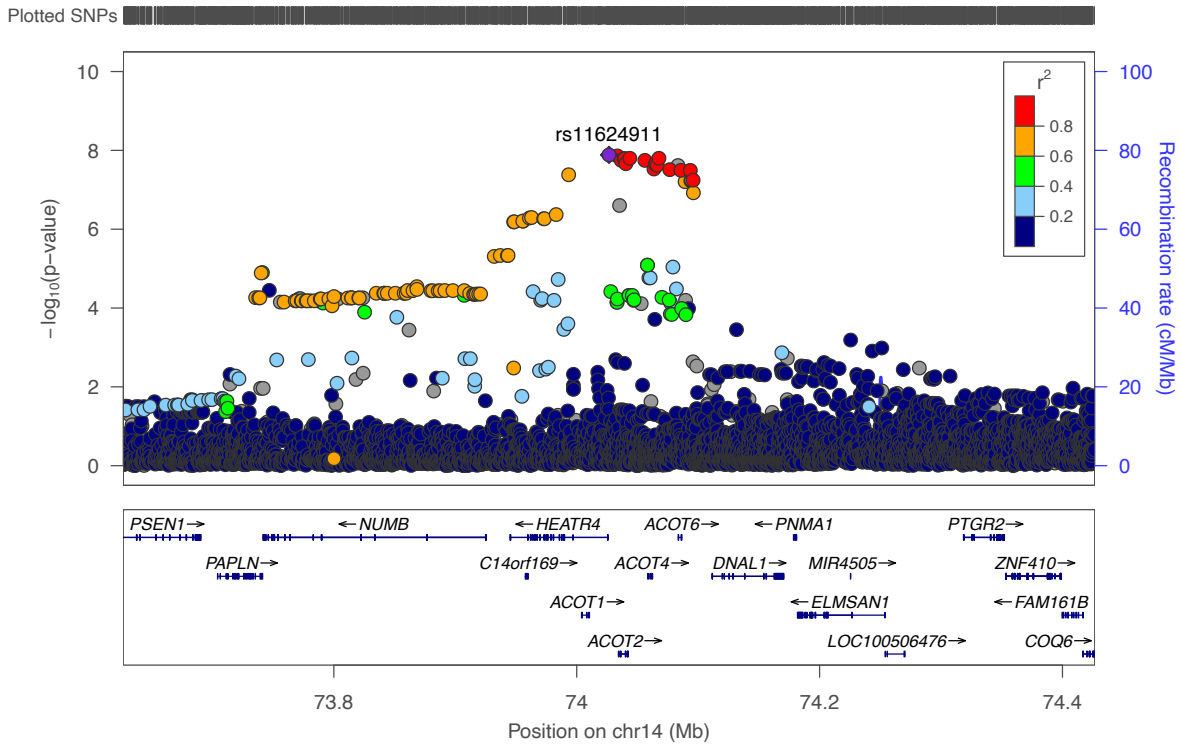

Supplemental Figure 9. Regional interrogation of the *UMOD/PDILT* locus from transethnic analyses among individuals without diabetes

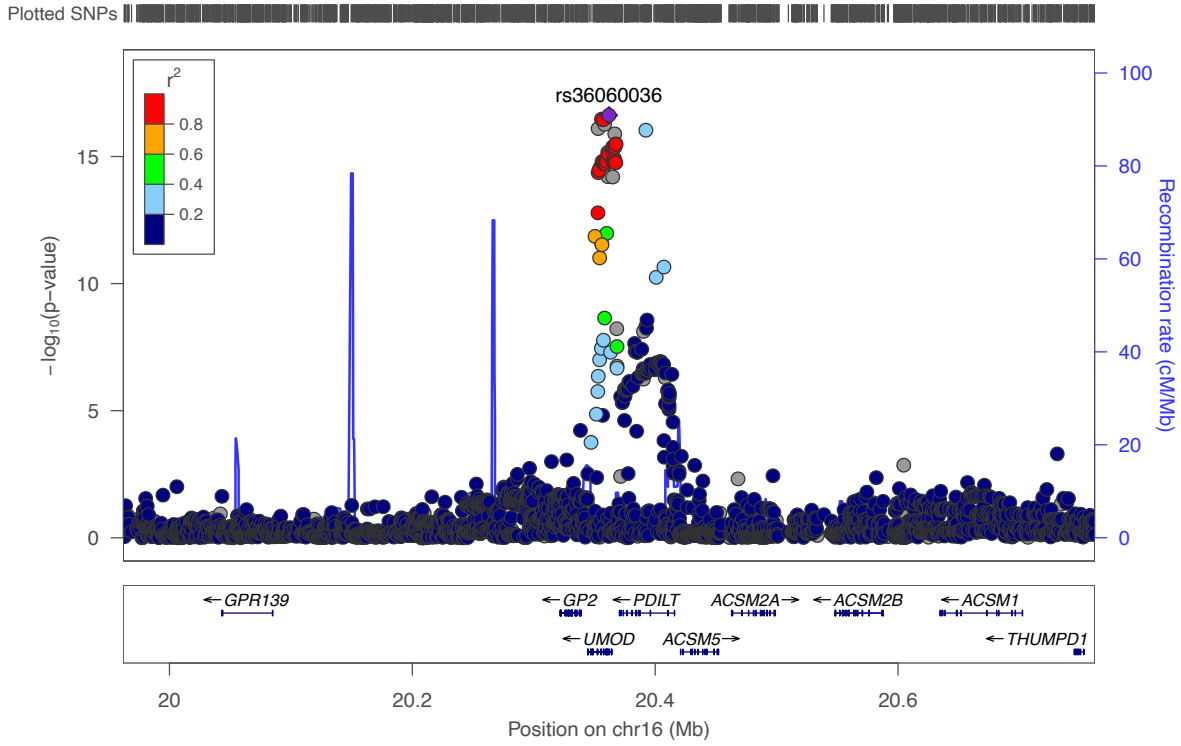

Supplemental Figure 10. Regional interrogation of the *BICC1* locus from cross-ancestry analyses among individuals without diabetes

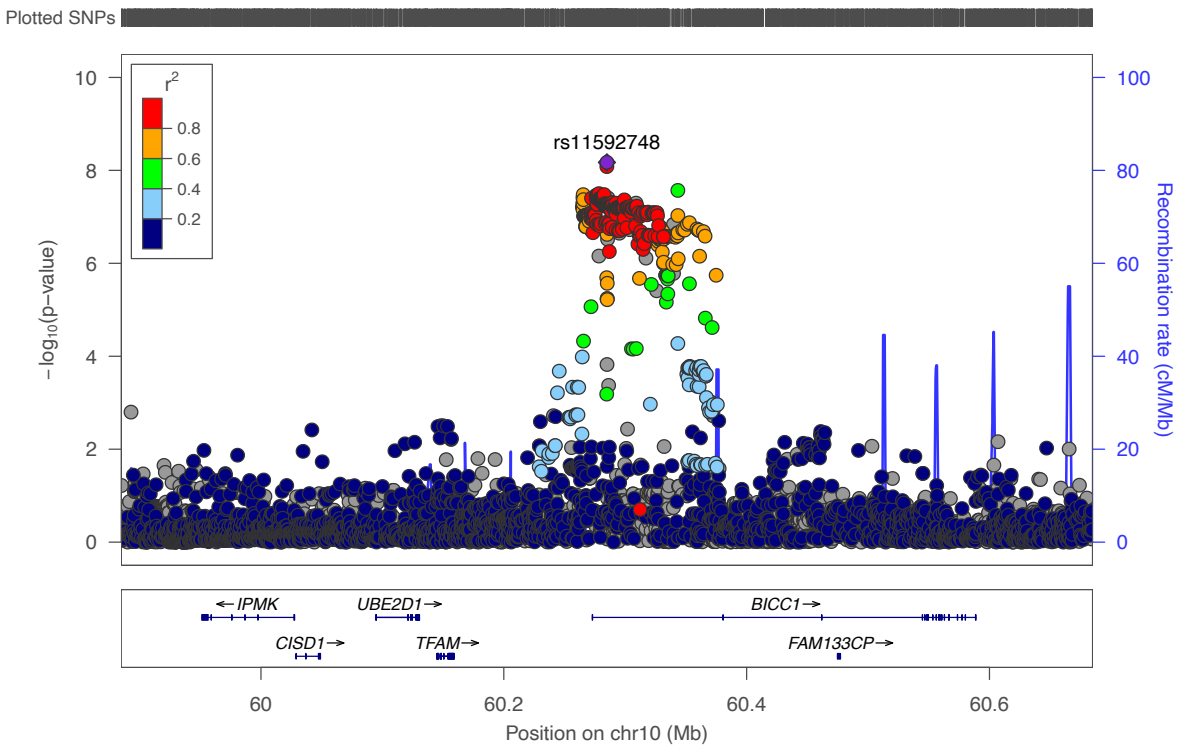

Supplemental Figure 11. Regional interrogation of the *PRKAG2* locus from cross-ancestry analyses

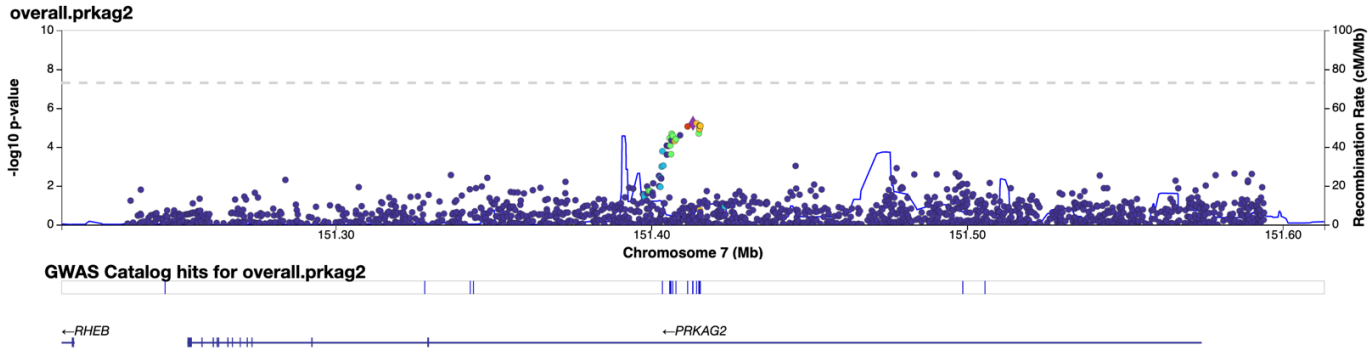

Supplemental Figure 12. Regional interrogation of the *FGF5* locus from cross-ancestry analyses

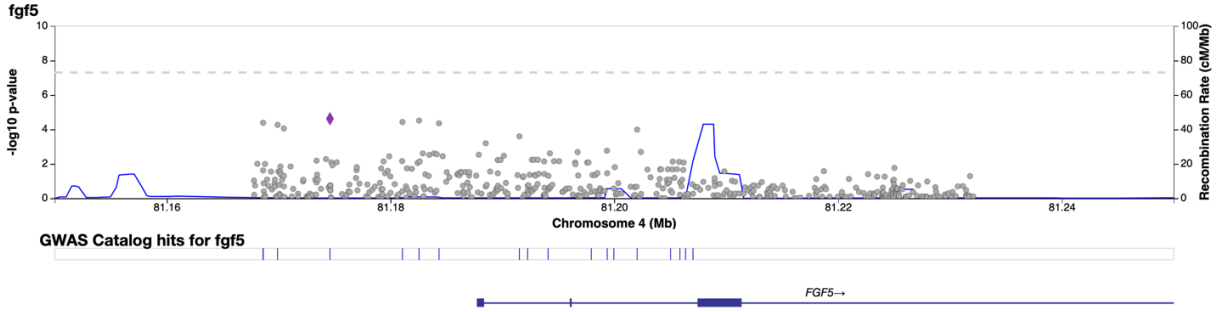

Supplemental Figure 13. Regional interrogation of the *C15ORF54* locus from cross-ancestry analyses

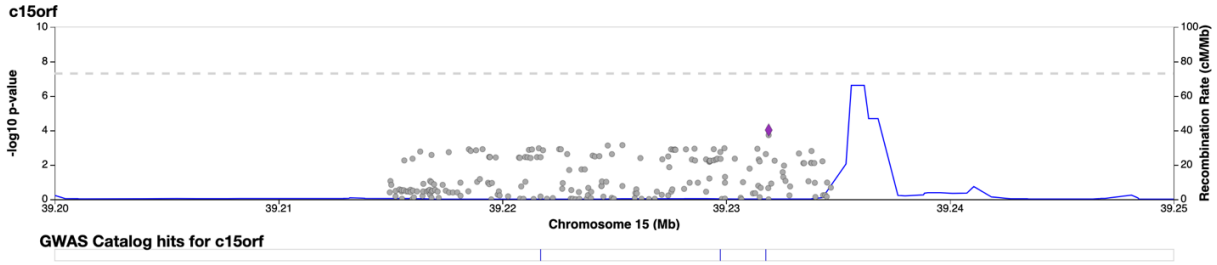

Supplemental Figure 14. Violin plots of distribution of relative eGFR by APOL1 inheritance model among Black participants with (A) and without (B) diabetes

A. Distribution of relative eGFR by *APOL1* inheritance model among Black participants with diabetes

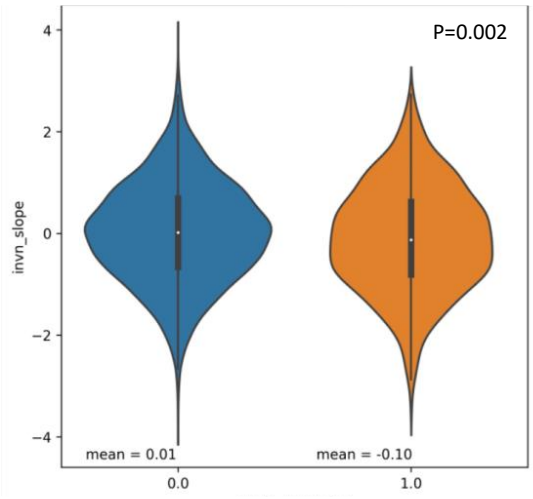

Recessive inheritance model
0 = 0-1 high-risk alleles
1 = 2 high-risk alleles

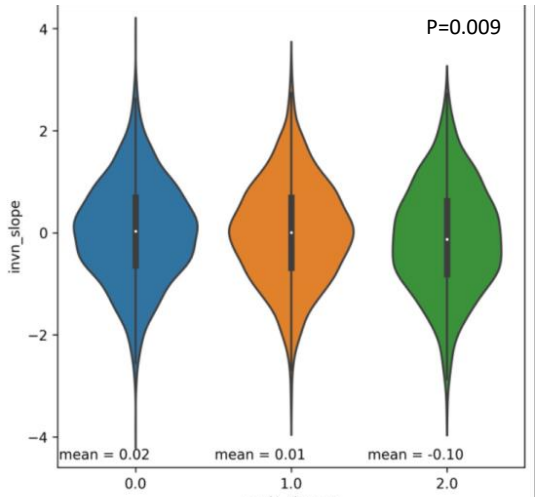

Additive inheritance model
0 = 0 high-risk alleles
1 = 1 high-risk allele
2 = 2 high-risk alleles

B. Distribution of relative eGFR by *APOL1* inheritance model among Black participants without diabetes

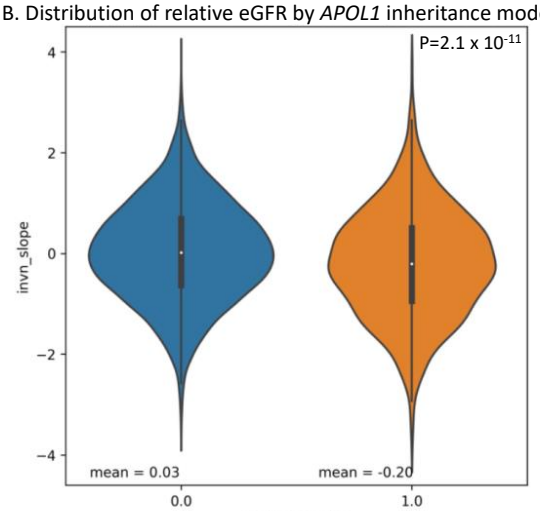

Recessive inheritance model
0 = 0-1 high-risk alleles
1 = 2 high-risk alleles

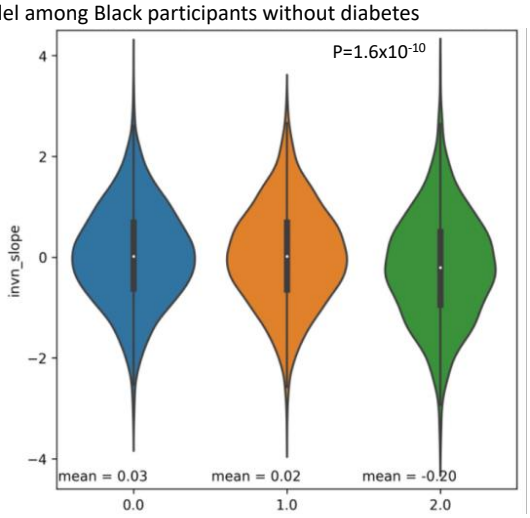

Additive inheritance model
0 = 0 high-risk alleles
1 = 1 high-risk allele
2 = 2 high-risk alleles

Supplemental Figure 15. Manhattan plot of the strength of association of genetic variants with eGFR decline (%/year) among White individuals with chronic kidney disease.

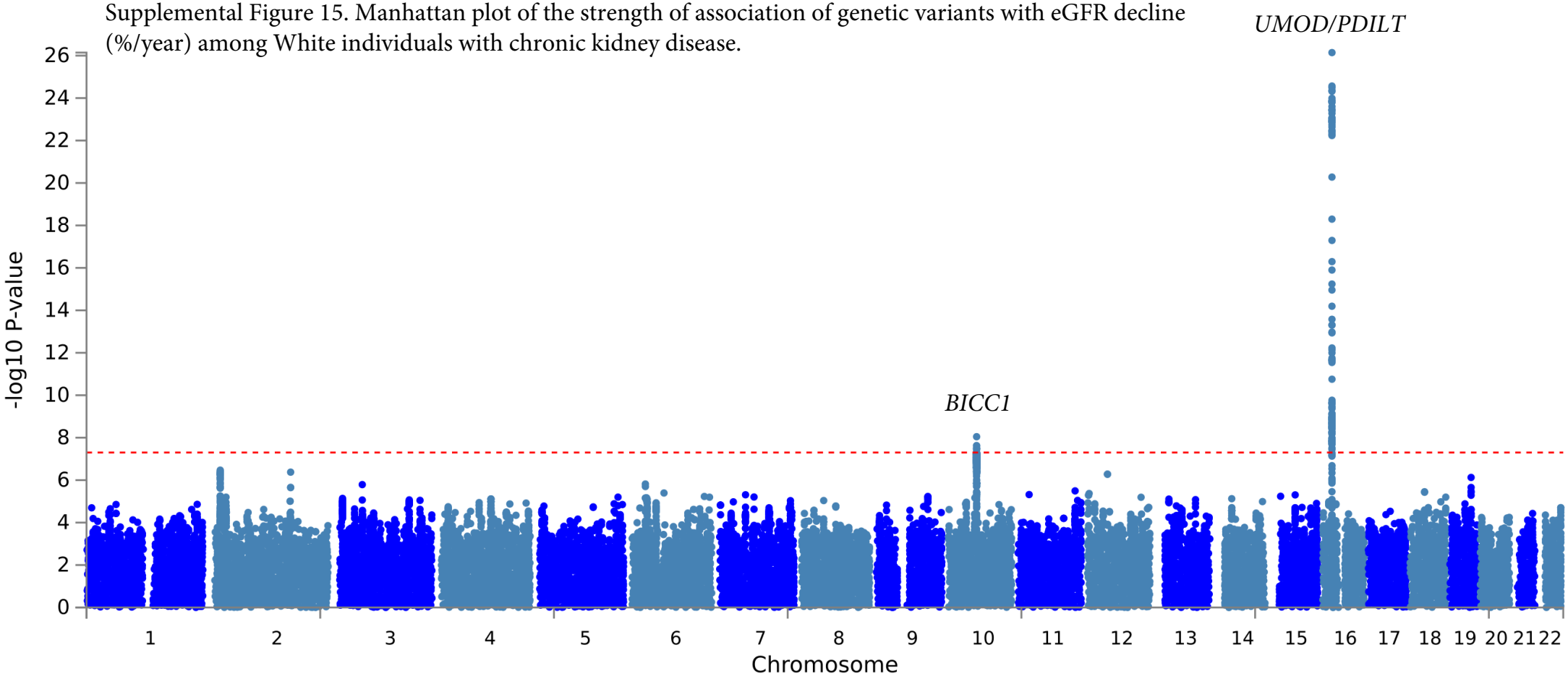

Supplemental Figure 16. Manhattan plot of the strength of association of genetic variants with eGFR decline (%/year) in among Black individuals with chronic kidney disease.

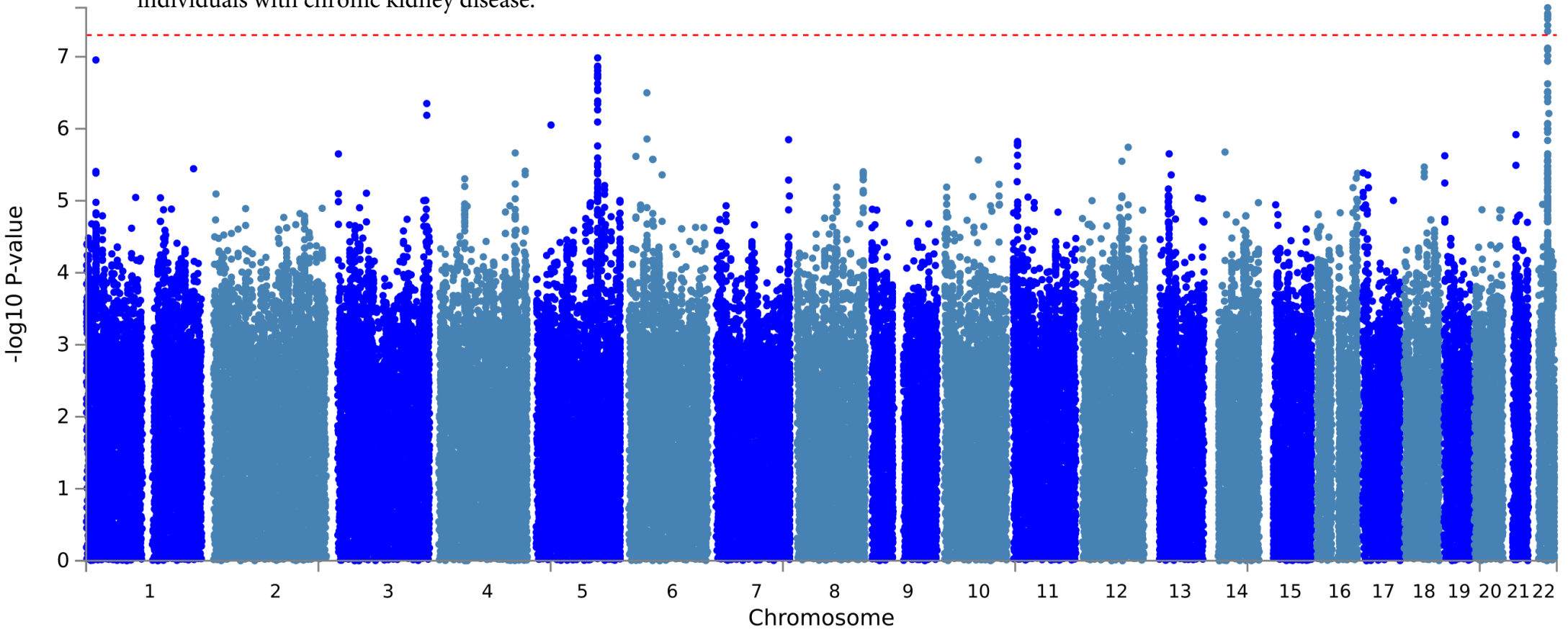

VA Million Veteran Program: Core Acknowledgement for Publications

Updated December 10, 2020

MVP Executive Committee

- Co-Chair: J. Michael Gaziano, M.D., M.P.H.
  VA Boston Healthcare System, 150 S. Huntington Avenue, Boston, MA 02130
- Co-Chair: Sumitra Muralidhar, Ph.D.
  US Department of Veterans Affairs, 810 Vermont Avenue NW, Washington, DC 20420
- Rachel Ramoni, D.M.D., Sc.D., Chief VA Research and Development Officer
  US Department of Veterans Affairs, 810 Vermont Avenue NW, Washington, DC 20420
- Jean Beckham, Ph.D.
  Durham VA Medical Center, 508 Fulton Street, Durham, NC 27705
- Kyong-Mi Chang, M.D.
  Philadelphia VA Medical Center, 3900 Woodland Avenue, Philadelphia, PA 19104
- Christopher J. O'Donnell, M.D., M.P.H.
  VA Boston Healthcare System, 150 S. Huntington Avenue, Boston, MA 02130
- Philip S. Tsao, Ph.D.
  VA Palo Alto Health Care System, 3801 Miranda Avenue, Palo Alto, CA 94304
- James Breeling, M.D., Ex-Officio
  US Department of Veterans Affairs, 810 Vermont Avenue NW, Washington, DC 20420
- Grant Huang, Ph.D., Ex-Officio
  US Department of Veterans Affairs, 810 Vermont Avenue NW, Washington, DC 20420
- Juan P. Casas, M.D., Ph.D., Ex-Officio
  VA Boston Healthcare System, 150 S. Huntington Avenue, Boston, MA 02130

MVP Program Office

- Sumitra Muralidhar, Ph.D.
  US Department of Veterans Affairs, 810 Vermont Avenue NW, Washington, DC 20420
- Jennifer Moser, Ph.D.
  US Department of Veterans Affairs, 810 Vermont Avenue NW, Washington, DC 20420

MVP Recruitment/Enrollment

- Recruitment/Enrollment Director/Deputy Director, Boston – Stacey B. Whitbourne, Ph.D.; Jessica V. Brewer, M.P.H.
  VA Boston Healthcare System, 150 S. Huntington Avenue, Boston, MA 02130
- MVP Coordinating Centers
  - Clinical Epidemiology Research Center (CERC), West Haven – Mihaela Aslan, Ph.D.
    West Haven VA Medical Center, 950 Campbell Avenue, West Haven, CT 06516

    - Cooperative Studies Program Clinical Research Pharmacy Coordinating Center, Albuquerque – Todd Connor, Pharm.D.; Dean P. Argyres, B.S., M.S.
      New Mexico VA Health Care System, 1501 San Pedro Drive SE, Albuquerque, NM 87108
    - Genomics Coordinating Center, Palo Alto – Philip S. Tsao, Ph.D.
      VA Palo Alto Health Care System, 3801 Miranda Avenue, Palo Alto, CA 94304
    - MVP Boston Coordinating Center, Boston - J. Michael Gaziano, M.D., M.P.H.
      VA Boston Healthcare System, 150 S. Huntington Avenue, Boston, MA 02130
    - MVP Information Center, Canandaigua – Brady Stephens, M.S.
      Canandaigua VA Medical Center, 400 Fort Hill Avenue, Canandaigua, NY 14424
- VA Central Biorepository, Boston – Mary T. Brophy M.D., M.P.H.; Donald E. Humphries, Ph.D.; Luis E. Selva, Ph.D.
  VA Boston Healthcare System, 150 S. Huntington Avenue, Boston, MA 02130
- MVP Informatics, Boston – Nhan Do, M.D.; Shahpoor (Alex) Shayan, M.S.
  VA Boston Healthcare System, 150 S. Huntington Avenue, Boston, MA 02130
- MVP Data Operations/Analytics, Boston – Kelly Cho, M.P.H., Ph.D.
  VA Boston Healthcare System, 150 S. Huntington Avenue, Boston, MA 02130
- Director of Regulatory Affairs – Lori Churby, B.S.
  VA Palo Alto Health Care System, 3801 Miranda Avenue, Palo Alto, CA 94304

MVP Science

- Science Operations – Christopher J. O'Donnell, M.D., M.P.H.
  VA Boston Healthcare System, 150 S. Huntington Avenue, Boston, MA 02130
- Genomics Core – Christopher J. O'Donnell, M.D., M.P.H.; Saiju Pyarajan Ph.D.
  VA Boston Healthcare System, 150 S. Huntington Avenue, Boston, MA 02130
  Philip S. Tsao, Ph.D.
  VA Palo Alto Health Care System, 3801 Miranda Avenue, Palo Alto, CA 94304
- Data Core – Kelly Cho, M.P.H, Ph.D.
  VA Boston Healthcare System, 150 S. Huntington Avenue, Boston, MA 02130
- VA Informatics and Computing Infrastructure (VINCI) – Scott L. DuVall, Ph.D.
  VA Salt Lake City Health Care System, 500 Foothill Drive, Salt Lake City, UT 84148
- Data and Computational Sciences – Saiju Pyarajan, Ph.D.
  VA Boston Healthcare System, 150 S. Huntington Avenue, Boston, MA 02130
- Statistical Genetics – Elizabeth Hauser, Ph.D.
  Durham VA Medical Center, 508 Fulton Street, Durham, NC 27705
  Yan Sun, Ph.D.
  Atlanta VA Medical Center, 1670 Clairmont Road, Decatur, GA 30033
  Hongyu Zhao, Ph.D.
  West Haven VA Medical Center, 950 Campbell Avenue, West Haven, CT 06516

Current MVP Local Site Investigators

- Atlanta VA Medical Center (Peter Wilson, M.D.)

1670 Clairmont Road, Decatur, GA 30033
- Bay Pines VA Healthcare System (Rachel McArdle, Ph.D.)
  10,000 Bay Pines Blvd Bay Pines, FL 33744
- Birmingham VA Medical Center (Louis Dellitalia, M.D.)
  700 S. 19th Street, Birmingham AL 35233
- Central Western Massachusetts Healthcare System (Kristin Mattocks, Ph.D., M.P.H.)
  421 North Main Street, Leeds, MA 01053
- Cincinnati VA Medical Center (John Harley, M.D., Ph.D.)
  3200 Vine Street, Cincinnati, OH 45220
- Clement J. Zablocki VA Medical Center (Jeffrey Whittle, M.D., M.P.H.)
  5000 West National Avenue, Milwaukee, WI 53295
- VA Northeast Ohio Healthcare System (Frank Jacono, M.D.)
  10701 East Boulevard, Cleveland, OH 44106
- Durham VA Medical Center (Jean Beckham, Ph.D.)
  508 Fulton Street, Durham, NC 27705
- Edith Nourse Rogers Memorial Veterans Hospital (John Wells., Ph.D.)
  200 Springs Road, Bedford, MA 01730
- Edward Hines, Jr. VA Medical Center (Salvador Gutierrez, M.D.)
  5000 South 5th Avenue, Hines, IL 60141
- Veterans Health Care System of the Ozarks (Gretchen Gibson, D.D.S., M.P.H.)
  1100 North College Avenue, Fayetteville, AR 72703
- Fargo VA Health Care System (Kimberly Hammer, Ph.D.)
  2101 N. Elm, Fargo, ND 58102
- VA Health Care Upstate New York (Laurence Kaminsky, Ph.D.)
  113 Holland Avenue, Albany, NY 12208
- New Mexico VA Health Care System (Gerardo Villareal, M.D.)
  1501 San Pedro Drive, S.E. Albuquerque, NM 87108
- VA Boston Healthcare System (Scott Kinlay, M.B.B.S., Ph.D.)
  150 S. Huntington Avenue, Boston, MA 02130
- VA Western New York Healthcare System (Junzhe Xu, M.D.)
  3495 Bailey Avenue, Buffalo, NY 14215-1199
- Ralph H. Johnson VA Medical Center (Mark Hamner, M.D.)
  109 Bee Street, Mental Health Research, Charleston, SC 29401
- Columbia VA Health Care System (Roy Mathew, M.D.)
  6439 Garners Ferry Road, Columbia, SC 29209
- VA North Texas Health Care System (Sujata Bhushan, M.D.)
  4500 S. Lancaster Road, Dallas, TX 75216
- Hampton VA Medical Center (Pran Iruvanti, D.O., Ph.D.)
  100 Emancipation Drive, Hampton, VA 23667
- Richmond VA Medical Center (Michael Godschalk, M.D.)
  1201 Broad Rock Blvd., Richmond, VA 23249

- Iowa City VA Health Care System (Zuhair Ballas, M.D.)
  601 Highway 6 West, Iowa City, IA 52246-2208
- Eastern Oklahoma VA Health Care System (Douglas Ivins, M.D.)
  1011 Honor Heights Drive, Muskogee, OK 74401
- James A. Haley Veterans' Hospital (Stephen Mastorides, M.D.)
  13000 Bruce B. Downs Blvd, Tampa, FL 33612
- James H. Quillen VA Medical Center (Jonathan Moorman, M.D., Ph.D.)
  Corner of Lamont & Veterans Way, Mountain Home, TN 37684
- John D. Dingell VA Medical Center (Saib Gappy, M.D.)
  4646 John R Street, Detroit, MI 48201
- Louisville VA Medical Center (Jon Klein, M.D., Ph.D.)
  800 Zorn Avenue, Louisville, KY 40206
- Manchester VA Medical Center (Nora Ratcliffe, M.D.)
  718 Smyth Road, Manchester, NH 03104
- Miami VA Health Care System (Hermes Florez, M.D., Ph.D.)
  1201 NW 16th Street, 11 GRC, Miami FL 33125
- Michael E. DeBakey VA Medical Center (Olaoluwa Okusaga, M.D.)
  2002 Holcombe Blvd, Houston, TX 77030
- Minneapolis VA Health Care System (Maureen Murdoch, M.D., M.P.H.)
  One Veterans Drive, Minneapolis, MN 55417
- N. FL/S. GA Veterans Health System (Peruvemba Sriram, M.D.)
  1601 SW Archer Road, Gainesville, FL 32608
- Northport VA Medical Center (Shing Shing Yeh, Ph.D., M.D.)
  79 Middleville Road, Northport, NY 11768
- Overton Brooks VA Medical Center (Neeraj Tandon, M.D.)
  510 East Stoner Ave, Shreveport, LA 71101
- Philadelphia VA Medical Center (Darshana Jhala, M.D.)
  3900 Woodland Avenue, Philadelphia, PA 19104
- Phoenix VA Health Care System (Samuel Aguayo, M.D.)
  650 E. Indian School Road, Phoenix, AZ 85012
- Portland VA Medical Center (David Cohen, M.D.)
  3710 SW U.S. Veterans Hospital Road, Portland, OR 97239
- Providence VA Medical Center (Satish Sharma, M.D.)
  830 Chalkstone Avenue, Providence, RI 02908
- Richard Roudebush VA Medical Center (Suthat Liangpunsakul, M.D., M.P.H.)
  1481 West 10th Street, Indianapolis, IN 46202
- Salem VA Medical Center (Kris Ann Oursler, M.D.)
  1970 Roanoke Blvd, Salem, VA 24153
- San Francisco VA Health Care System (Mary Whooley, M.D.)
  4150 Clement Street, San Francisco, CA 94121
- South Texas Veterans Health Care System (Sunil Ahuja, M.D.)

7400 Merton Minter Boulevard, San Antonio, TX 78229
- Southeast Louisiana Veterans Health Care System (Joseph Constans, Ph.D.)
  2400 Canal Street, New Orleans, LA 70119
- Southern Arizona VA Health Care System (Paul Meyer, M.D., Ph.D.)
  3601 S 6th Avenue, Tucson, AZ 85723
- Sioux Falls VA Health Care System (Jennifer Greco, M.D.)
  2501 W 22nd Street, Sioux Falls, SD 57105
- St. Louis VA Health Care System (Michael Rauchman, M.D.)
  915 North Grand Blvd, St. Louis, MO 63106
- Syracuse VA Medical Center (Richard Servatius, Ph.D.)
  800 Irving Avenue, Syracuse, NY 13210
- VA Eastern Kansas Health Care System (Melinda Gaddy, Ph.D.)
  4101 S 4th Street Trafficway, Leavenworth, KS 66048
- VA Greater Los Angeles Health Care System (Agnes Wallbom, M.D., M.S.)
  11301 Wilshire Blvd, Los Angeles, CA 90073
- VA Long Beach Healthcare System (Timothy Morgan, M.D.)
  5901 East 7th Street Long Beach, CA 90822
- VA Maine Healthcare System (Todd Stapley, D.O.)
  1 VA Center, Augusta, ME 04330
- VA New York Harbor Healthcare System (Scott Sherman, M.D., M.P.H.)
  423 East 23rd Street, New York, NY 10010
- VA Pacific Islands Health Care System (George Ross, M.D.)
  459 Patterson Rd, Honolulu, HI 96819
- VA Palo Alto Health Care System (Philip Tsao, Ph.D.)
  3801 Miranda Avenue, Palo Alto, CA 94304-1290
- VA Pittsburgh Health Care System (Patrick Strollo, Jr., M.D.)
  University Drive, Pittsburgh, PA 15240
- VA Puget Sound Health Care System (Edward Boyko, M.D.)
  1660 S. Columbian Way, Seattle, WA 98108-1597
- VA Salt Lake City Health Care System (Laurence Meyer, M.D., Ph.D.)
  500 Foothill Drive, Salt Lake City, UT 84148
- VA San Diego Healthcare System (Samir Gupta, M.D., M.S.C.S.)
  3350 La Jolla Village Drive, San Diego, CA 92161
- VA Sierra Nevada Health Care System (Mostaqul Huq, Pharm.D., Ph.D.)
  975 Kirman Avenue, Reno, NV 89502
- VA Southern Nevada Healthcare System (Joseph Fayad, M.D.)
  6900 North Pecos Road, North Las Vegas, NV 89086
- VA Tennessee Valley Healthcare System (Adriana Hung, M.D., M.P.H.)
  1310 24th Avenue, South Nashville, TN 37212
- Washington DC VA Medical Center (Jack Lichy, M.D., Ph.D.)
  50 Irving St, Washington, D. C. 20422

- W.G. (Bill) Hefner VA Medical Center (Robin Hurley, M.D.)
  1601 Brenner Ave, Salisbury, NC 28144
- White River Junction VA Medical Center (Brooks Robey, M.D.)
  163 Veterans Drive, White River Junction, VT 05009
- William S. Middleton Memorial Veterans Hospital (Robert Striker, M.D., Ph.D.)
  2500 Overlook Terrace, Madison, WI 53705